CHAPTER 262

Small-scale Morphology Related to Wave and Current Parameters Over a Barred Beach

A.F. Garcez Faria[1], E.B. Thornton[1], T.P. Stanton[1]

ABSTRACT: Small-scale morphology (< 5 m horizontal wavelength) was measured by combining CRAB surveys with bed elevations acquired from a 1 MHZ sonic altimeter mounted on the CRAB during the DUCK94 experiment in October 1994. Bedform plan views were recorded simultaneously using a 500 KHz side-scan sonar mounted on the CRAB. Waves and currents were measured at the same time. Three cases are examined in detail: mild waves and weak longshore currents resulting in wave ripples throughout the study area; narrow-band, normally incident waves with a strong rip current resulting in a planar bed except in the throat of the rip where mega-ripples were measured; and storm waves with strong longshore currents resulting in lunate and straight-crested mega-ripples in the trough of the barred beach. During these strong current days, bed shear stresses calculated from logarithmic velocity profiles are equated to a quadratic bottom shear stress formulation. The associated bed shear stress coefficients vary by more than an order of magnitude across the surf zone (0.0006-0.012). Bottom roughness was obtained by calculating the wavenumber spectra of the bed. The bed shear stress coefficients are positively correlated with bottom roughness (linear correlation coefficient, 0.68). A higher linear correlation coefficient (0.80) is obtained by subtracting skin friction from the total bed shear stress.

INTRODUCTION

The nearshore bed on a barred beach is composed of complex bedforms caused by varying wave and current regimes. With the exception of wave ripples in deeper water, few quantitative observations of bedforms are available, especially in the nearshore, and simultaneous quantitative wave and current measurements are almost non-existent. The lack of data is due to difficulties in making measurements in the nearshore. Observations historically have been made by divers who are limited by visibility and the harsh nearshore environment, which can become unfavorable for observations even in the mildest of storms.

Earlier field measurements were reported by Dingler and Inman (1976), which profiled wave ripples using a moveable acoustic altimeter placed on a track on the bottom outside the surf zone, but were limited to a single track of approximately 2 m in length. Other methods have included using waxed combs pushed into the bed by divers to record ripple profiles. Miller and Komar (1980) found ripple wavelength to be related to the orbital diameter of the waves.

The measurements described in this paper were made in shallow water (<8m) where shoaling and breaking waves are typically asymmetric, resulting in asymmetric bedforms. A conceptual view of wave-induced small-scale morphology on a barred beach is summarized by Clifton (1976) based on diver observations, which describes the asymmetric transition of bedforms with increasing velocity from long-crested

---

[1]Oceanography Department, Naval Postgraduate School, Monterey, CA, 93943-5000, USA; E-mail: faria@oc.nps.navy.mil; Tel: +1 408 656 2379; Fax: +1 408 656 2712.

ripples, to irregular ripples, to cross-ripples, to lunate mega-ripples on the seaward slope of the bar, to a planar bar crest where the waves break, and to wave ripples again in the trough where wave intensity decreases after waves cross the bar. These are the least observed nearshore bedforms owing to difficulties in obtaining quantitative measurements.

The objective of this paper is to correlate small-scale morphology measured over a barred beach with waves and currents. In the following sections, a description of the DUCK94 experiment, the methodology of the data analysis, the description of the small-scale morphology observed on Oct. 8, 12, and 20, and the relationship between measured bottom roughness and bed shear stress are presented.

DUCK94 EXPERIMENT

The measurements described here are part of the comprehensive nearshore DUCK94 experiment conducted during October 1994 at the U.S. Army Corps of Engineers Field Research Facility (FRF), Duck, North Carolina. The weather during October was climatologically characterized by three distinct phases: weak currents and winds from the north (4-9 Oct.), relatively strong currents from the north (0.6-1.0 m/s) caused by a storm with predominant winds and waves from the north (10-12 Oct.), and variable currents and winds from the north/south (13-21 Oct.).

The morphology of the bottom (bathymetry) was measured at various scales using the Coastal Research Amphibious Buggy (CRAB). The surveys were performed daily during the experiment by driving the CRAB in a series of cross-shore survey lines with alongshore separation of 25 to 30m. Large-scale variations of bathymetry were obtained by recording the CRAB position using a laser ranging/auto-tracking system approximately every meter (order 3 cm rms vertical and horizontal accuracy). Three-dimensional, large-scale morphology mapped by the CRAB during the three periods of interest (8, 12, and 20 Oct.) are shown in Fig. 1.

Small-scale vertical bottom variations relative to the CRAB, including ripples and megaripples, were measured with a 1 MHZ sonic altimeter mounted on the CRAB 70 cm from the bed. The altimeter has a nominal sampling rate of 25 Hz, which resulted in a sample spacing of 2-4 cm (dependent on CRAB speed) with mm vertical resolution and accuracy less than 2 cm (Gallagher *et al.*, 1995). The decrease in accuracy relative to resolution is due to the changing reflective surface owing to the bed dialating or sediment transported along the bed as waves pass overhead. The CRAB survey and altimeter measurements were combined to obtain a high resolution description of the bottom (Thornton *et al.*, 1996).

A 500 KHz side-scan sonar suspended in the center of the CRAB approximately 1.25 m from the bed generates high-resolution plan views of the morphology. The nominal horizontal range of the sonar was approximately 10 to 15 m to each side of the sonar, which allowed overlap of sonar data from adjacent survey lines, giving a relatively complete view of the geometry and spatial representation of the ripple features.

Corroborating wave and current data were acquired using an instrumented sled. A vertical stack of eight Marsh-McBirney two-component electromagnetic

current meters (em's, hereafter) with 2.5 cm diameter spherical probes were mounted on a 2.5 m mast to measure vertical profiles of longshore and cross-shore currents. The sled was oriented with the vertical stack of current meters placed on the up-eurrent side to prevent the sled structure from contaminating flow measurements. Waves and mean water level were measured using an array of five pressure sensors configured in a 3 m square with sensors at the corners and one at the center. For data collection, each morning the sled was towed by the CRAB to its furthest position offshore, dependent upon wave conditions, for the first data run. A forklift on the beach pulled the sled shoreward approximately 10 to 30 m for each subsequent run. Data were acquired at each location for approximately one hour at four to eight locations. Additionally, directional wave spectra were acquired using a linear array of 10 pressure sensors in 8 m depth offshore of the survey area.

METHODOLOGY

The bottom roughness is examined by calculating wavenumber spectra of the bed. To calculate wavenumber spectra, the unevenly spaced data from the combined CRAB surveys and altimeter measurements are linearly interpolated to evenly spaced 2 cm increments of the cross-shore distance. The small-scale morphology in general shows large cross-shore variation; as a consequence, the condition of spatial homogeneity (stationarity) required for calculating averaged spectra is not met. Therefore, continuous wavenumber spectra are calculated for 20 m cross-shore segments at increments of 1 m across the surf zone. Lowest wave numbers are filtered by subtracting a third-order polynomial best-fit curve from each 20 m section. A 10 percent eosine-taper data window is applied. The spectra are summed over three wavelength bands (0.4 - 0.83 m, 0.83 - 1.67 m, and 1.67 - 5 m) plus the total band (0.4 - 5 m), resulting in 52, 24, 16, and 92 degrees of freedom for each band respectively. The wavelength bands chosen are based on examination of individual spectra that were generally broad, indicating that several ripple wavelengths coexisted as a result of newly formed ripples combining with residual ripples from the past to form a complex series of ripple patterns. The *rms* height of each band is calculated as the square root of the variance within each band.The general trend is that the bottom was smoothest offshore and over the bar where wave ripples were planed-off due to higher near-bottom velocities, with increased roughness within the trough associated with mega-ripples (see Thornton, *et al.*, 1996, for details).

Linear shear stress gradients occur in flows driven by constant hydrostatic pressure gradients, such as in steady open channel flows, are well described by a logarithmic velocity profile. Therefore it is hypothesized that a steady, uniform, turbulent boundary layer flow over a rough surface in the alongshore direction can be described by a logarithmic profile:

$$V(z) = \frac{v_*}{\kappa} \ln \left(\frac{z + h}{z_o}\right) \qquad (1)$$

where z is positive upwards from the surface, h is the mean water depth, κ is the Von Karman constant (0.4), v_* is the alongshore shear stress velocity and z_o is the physical roughness height, determined by bottom topography and sediment grain size. When waves are present, nonlinear interactions between waves and currents within the bottom boundary layer increase the bottom shear stress. Following Grant and Madsen (1979), this additional stress can be modeled by an apparent roughness height z_a, that is analogous to, but larger than z_o. Logarithmic profiles are fit to the data based on a linear-regression least-squares method. The value of z_a is calculated from the z intercept of the linear-regression on a semi-log plot of z versus V(z), and the shear stress velocity v_* is calculated from the slope.

Mean along shore bottom shear stress ($\overline{\tau_y(-h)}$) is related to the alongshore shear stress velocity (v_*) through (overbar indicates time averaging)

$$\overline{\tau_y(-h)} = \rho v_*^2 \tag{2}$$

where ρ is water density. In addition, the bed shear stress coefficient, C_f, can be calculated assuming a quadratic bed shear stress relationship

$$\overline{\tau_y(-h)} = \rho C_f \overline{(u^2 + v^2)^{1/2} v} \tag{3}$$

and combining with (2), gives

$$C_f = \frac{v_*^2}{\overline{(u^2 + v^2)^{1/2} v}} \tag{4}$$

C_f values are calculated using measured velocities (u,v) at the elevation of 1 m above the bed, with v_* determined by least-squares log fit (Garcez Faria *et al.*, 1996).

DISCUSSION

October 8 Morphology

The large-scale morphology on Oct. 8 at first glance appears to be relatively homogeneous. The offshore bar is nearly parallel to the shore and is located approximately 230-250 m offshore (Fig. 1). Therefore, it would be expected that the small-scale morphology would also be homogenous alongshore throughout the survey area given the same wave and current conditions. However, close examination shows that the small-scale morphology is not homogeneous and that ripple patterns vary both in the cross-shore and alongshore directions.

Two representative lines (710 and 940 m along shore coordinate) of cross-shore combined CRAB and altimeter profiles are selected to depict the differences present in the small-scale morphology for the survey area (Fig. 2). The primary differences in the ripple dimensions between the two representative lines are observed in the trough and the seaward slope of the bar. The small-scale morphology in the trough of line 940 is predominantly long wavelength mega-ripples (1.67-5 m)

with shorter wavelength wave ripples superimposed on them. The trough region of line 710 has a more homogeneous ripple pattern in which no wavelength band predominates. The seaward slope of the bar on line 940 shows the ripple wavelength bands of 0.83-1.67 m and 1.67-5 m are dominant and the rms height is on the order of 3 cm. The seaward slope of the bar on line 710 shows relatively homogeneous ripple wavelengths with rms heights of approximately 2 cm.

October 20 Morphology

The most striking observation on the 20th is the hole in the bar with the bar bowed seaward due to the rip current between 800 and 1100 m in alongshore coordinates (Fig. 1). The bar is parallel to the beach and is located approximately 210-225 m offshore north of the rip area, shifting to greater than 300 m offshore in the rip area. The narrow trough, north of the rip area, acts as a rip-feeder channel and has the same small-scale morphological features as the rip area. The dominant small-scale morphology observed in the rip area are seaward-facing lunate and straight-crested mega-ripples. The mega-ripples were generally asymmetric with the steep slope facing seaward indicating the ripples were formed primarily as a result of the rip current. However, some ripples were symmetric while others were asymmetric facing toward the beach, which may infer a more complex formation due to a combination current and wave interactions. The area immediately north and south of the rip current is void of any discernable small-scale morphology with the exception of the rip-feeder channel. Typical rms roughness values in the rip area range from 5 to 15 cm, which are an order of magnitude larger than rms roughness values away from the rip. A contour plot of rms roughness values for the survey area is shown in Fig. 3, which displays the extreme variability of roughness in the rip current area compared with that of the area away from the rip current. The rip current, as qualitatively observed with dye on the 20th, is superimposed on the accompanying contour plot of the macro-scale bathymetry. The bed is essentially smooth away from the rip current with rms roughness values being less than 2 cm, which appears to be the result of planing action of the long-period swell.

October 12 Morphology

The large-scale morphology of Oct. 12 is similar to that of Oct. 8. The offshore bar is nearly parallel to the beach, but migrated 30 m offshore to approximately 260-280 m offshore (Fig. 1). Although the large-scale morphology is similar for the two days, the small-scale morphology is dramatically different owing to differences in the wave and current conditions associated with the arrival of a storm on Oct. 10. Large amplitude mega-ripples are now present in the trough and no regular bedform patterns are observed seaward of the bar for the entire survey area. The strong longshore current that appeared on the 10th is believed to be the dominant process that formed the small-scale morphology observed in the trough on the 12th.

The small-scale morphology across the surf zone is relatively homogeneous alongshore, and therefore, the survey area is represented by the rms roughness from the combined CRAB and altimeter profile for line 940 (Fig. 4, lower panel), which

is close to the position occupied by the sled. The small-scale morphology in the trough compared with the region seaward of the bar crest are distinctly different. Seaward of the bar the bed is essentially plane, due to intense breaking associated with large waves. In the trough, the rms roughness is primarily associated with the larger ripple wavelengths of 1.67-5 m. Side scan plots showed the mega-ripples in the outer trough to be lunate, facing in the direction of the longshore current; while straight crested in the inner trough.

Bottom Roughness and Bed Shear Stress

The more energetic period (Oct 10-12) is used to relate small-scale morphology to wave and current forcing. The data are qualitatively sorted by location into the two regions of over the bar and in the trough. This sorting allows a better identification of the possible correlations among variables, as wavc breaking which is a major controlling factor within the surf zone is significantly different for these regions.

All 22 vertical profiles of longshore currents obtained during these three days are analyzed. The profiles are based on the measurements by three to seven em's over the vertical. The em closest to the sea bed was not used because of malfunction. The observed and logarithmic predicted velocity profiles at successive offshore positions (runs) that the sled occupied during 12 Oct. is shown in the upper panel of Fig 4. The data agree well with the model.

A high correlation coefficient for the linear regression, is commonly accepted as an indicator of the validity of the logarithmic approach (Gross *et al.*, 1994; Li, 1994). The linear correlation coefficients for all profiles ranged from 0.95 to 0.99, with an average value of 0.98, and the largest deviations occurring over the bar, where wave breaking was strong.This can be related to the increase of turbulent mixing due to wavc breaking producing a more uniform vertical profile of the current for a given shear stress, compared with profiles in the absence of breaking. Therefore, larger discrepancies between observations and logarithmic profile predictions (lower correlation coefficients) would be expected for increased turbulent mixing caused by wave breaking, as the logarithmic profile presumes no surface turbulence source.

The bottom shear stress coefficient (C_f) varied by an order of magnitude across the surf zone, with the values offshore and over the bar in the order of 10^{-3}, while the values in the trough were in the order of 10^{-2}. An attempt was made to find empirical relationships between C_f with measured physical parameters commonly used throughout the literature such as $|\vec{u}_b| \ / \ V$ (ratio of near-bottom wave velocity magnitude to mean current speed), and the *rms* bottom roughness (r). Surprisingly, no statistically significant correlation was found between C_f and $|\vec{u}_b| \ / \ V$. The strongest correlation was found between C_f and the bottom roughness, with C_f increasing with bottom roughness (Fig. 5, upper panel), with a linear correlation coefficient of 0.68, which is statistically significant at the 99.75 percent confidence level. Theoretically this is expected as larger roughness implies larger bottom stress due to form drag, and consequently larger C_f values.

The scatter of data observed in Fig. 5 (upper panel) may be due to correlating the non-synoptic velocity measurements with bottom roughness measured once in the

morning, prior to the positioning of the sled for the first station. Wave forcing changed during the period of observation due to both wind and tidal variations. Changes in wave forcing have a direct effect in the measured velocities and an indirect effect in bottom roughness due to modification of wave ripples associated with variations in wave height.

Another reason for scatter of data arises from C_f values being calculated from the total bottom shear stress, which has stress contributions from skin friction related to sediment grains, waves-current nonlinear interactions within the bottom boundary layer as well as form drag related to bed forms. Smith and McLean (1977) linearly partitioned the total bed shear stress into skin friction and form drag and found good agreement with the data from the Columbia River. Extending this concept to the surf zone environment requires adding a component due to non-linear interactions between waves and currents within the bottom boundary layer to the total bed shear stress. Assuming that the linear stress partition is valid within the surf zone, the skin friction contribution can be removed from the total bottom stress and a new bed shear stress coefficient $C_f^{/}$ is defined

$$C_f^{/} = \frac{v_{*_d}^{\,2} + v_{*_{wc}}^{\,2}}{(u^2 + v^2)^{1/2} v} \tag{5}$$

where v_{*_d} and $v_{*_{wc}}$ are the form drag and waves-current interactions shear stress velocities. The relationship between $C_f^{/}$ and the total bed shear stress coefficient (C_f) can be determined from (4) and (5)

$$C_f^{/} = [1 - (\frac{v_{*_s}}{v_*})^2] \, C_f \tag{6}$$

where v_{*_s} is the skin friction related shear stress velocity. As skin friction was not measured during the DUCK94 experiment, an attempt is made to isolate its contribution from the total bottom shear stress by applying a stress partitioning model. The probabilistic approach used to quantify bottom roughness does not allow the adjustment of the two empirical coefficients C_D and a_1 necessary to apply the Smith and McLean (1977) model. Therefore, the empirical relationships obtained by Li (1994) are used to estimate skin friction shear stress velocity from the total shear stress velocity obtained from the logarithmic profile

$$\frac{v_{*_s}}{v_*} = 0.125(\frac{v_*}{R}) + 0.373 \qquad for \quad \frac{v_*}{R} < 2.3 \; s^{-1} \tag{7}$$

$$\frac{v_{*_s}}{v_*} = 0.107\left(\frac{v_*}{R}\right) + 0.266 \quad for \quad \frac{v_*}{R} \geq 2.3\ s^{-1} \tag{8}$$

where R is ripple height, assumed here to be equal to the measured *rms* bottom roughness ($R = r$) . The recalculated bed shear stress coefficients C_f' (Equation 6) are also positively correlated with bottom roughness (Fig. 5, lower panel), but show a higher linear correlation coefficient (0.80). Theoretically this is expected as the removal of the skin friction component from the total stress should enhance the form drag contribution, and consequently increase the correlation between bed shear stress and bottom roughness.

CONCLUSIONS

Quantitative measurements of small-scale morphology on a barred beach were acquired during the DUCK94 experiment. Three separate sequences are examined in which distinctly different ripple dimensions and bedform types were observed owing to varying wave and current regimes.

The measurements of small-scale morphology on Oct. 8, when mild waves and weak longshore currents prevailed, shows surprising differences within the survey area. The absence of significant variation associated with wave and current forcing suggests that the mega-ripples in the trough of line 940 may be residual from some earlier time of formation, such as on Oct. 3 when a strong longshore current was present.

Oct. 20 is characterized by a rip current with two distinct areas of small-scale morphology. In the throat of the rip current, straight-crested and lunate mega-ripples were observed. The area away from the rip current was void of any ripple patterns as a result of the planing action of the long-period swell.

Oct. 12 is characterized by the occurrence of a strong longshore current. The small-scale morphology of the inner trough region is characterized by relatively straight-crested mega-ripples (1.67-5 m) generated by the waves, superimposed by smaller wavelength ripples O(1 m). In the outer trough, lunate mega-ripples in the direction of the longshore current predominated. Seaward of the bar, the bed was essentially void of ripples.

The wavenumber spectral results infer a spatial and temporal variability of ripple dimensions in both the cross-shore and alongshore directions. The wavenumber spectra were generally broad, indicating that several ripple wavelengths coexisted as a result of newly formed ripples combined possibly with residual ripples from the past to form a complex series of ripple patterns. This broadening is also due to non-cross-shore (cross-track) orientation of the morphological features.

The vertical structure of mean longshore currents on a barred beach is well described by a logarithmic profile for the three strong longshore current days examined. This hypothesis works better in the trough where turbulent bottom boundary layer processes are more dominant than over the bar, where breaking-wave induced turbulence generated at the surface modifies the profile.

A relationship between bed shear stress coefficients (C_f) and bottom roughness was found. While the relatively small amount of data used (three days) are not enough to establish a definitive empirical relation from the available data, it can be concluded that C_f is directly proportional to bottom roughness, and therefore, the latter is an important parameter to characterize the bottom boundary layer. Surprisingly, only poor correlations of C_f and z_a were found with wave parameters.

The empirical relationships obtained by Li (1994) were used to remove the skin friction contribution from the total bottom shear stress. The improved correlation between bottom shear stress and bottom roughness obtained, although not conclusive to validate these simple expressions, indicates that the linear stress partition concept introduced by Smith and McLean (1977) can be extended to the surf zone environment.

ACKNOWLEDGMENTS

This research was funded by the Office of Naval Research, Coastal Sciences Program, under contract N00114-95-AF-002. The authors wish to express their appreciation to all those who participated in DUCK94 experiment, particularly the staff of the U.S. Army Field Research Facility. In addition, special appreciation is expressed to R. Wyland, Jim Stockel, and Mary Bristow, Naval Postgraduate School, for their role in the acquisition and processing of wave and current data.

REFERENCES

Clifton, H.E. (1976) "Wave-formed sedimentary structures- A conceptual model." *Beach and Nearshore Sedim., SEPM, Special Publication*, 24, 126-148.

Dingler, J.R., and Inman, D.L. (1976) "Wave formed ripples in the seashore sands." *Proceedings 15th Coastal Engineering Conference, ASCE*, pp. 2109-2126.

Gallagher, E.L., Boyd, W., Elgar, S., Guza, R.T., and Woodward, B. (1996). "A performance of a sonar altimeter in the nearshore." *Marine Geology*, 133, 241-248.

Garcez Faria, A.F., Thornton, E.B., Stanton, T. P., and Soares, C.M.C.V. (1996) "Vertical profiles of longshore currents and related bed shear stress and bottom roughness." *J. of Geophysical Research*, (submitted).

Grant, W.D., and Madsen, O.S. (1979) "Combined wave and current interaction with a rough bottom." *J. of Geophysical Research*, 84 (C4), 1797-1808.

Gross, T.F., Williams III, A.J., and Terray, E.A. (1994) "Bottom boundary layer spectral estimates in the presence of wave motions." *Continental Shelf Research*, 14, 1239-1256.

Li, M.Z. (1994) "Direct skin friction measurements and stress partitioning over movable sand ripples." *Journal of Geophysical Research*, 99(C1), 791-799.

Miller, M.C., and Komar, P.D. (1980) "A field investigation between oscillation ripple spacing and the near-bottom water orbital motions." *J. Sedimentary Petrology*, 50, 180-191.

Smith, J.D., and McLean, S.R. (1977) "Spatially averaged flow over a wavy surface." *Journal of Geophysical Research*, 82(C12), 1735-1746.

Thornton, E.B., Swayne, J.L., and Dingler, J.R. (1996) "Small-scale morphology related to waves and currents across the surf zone." *Mar. Geology* (accepted).

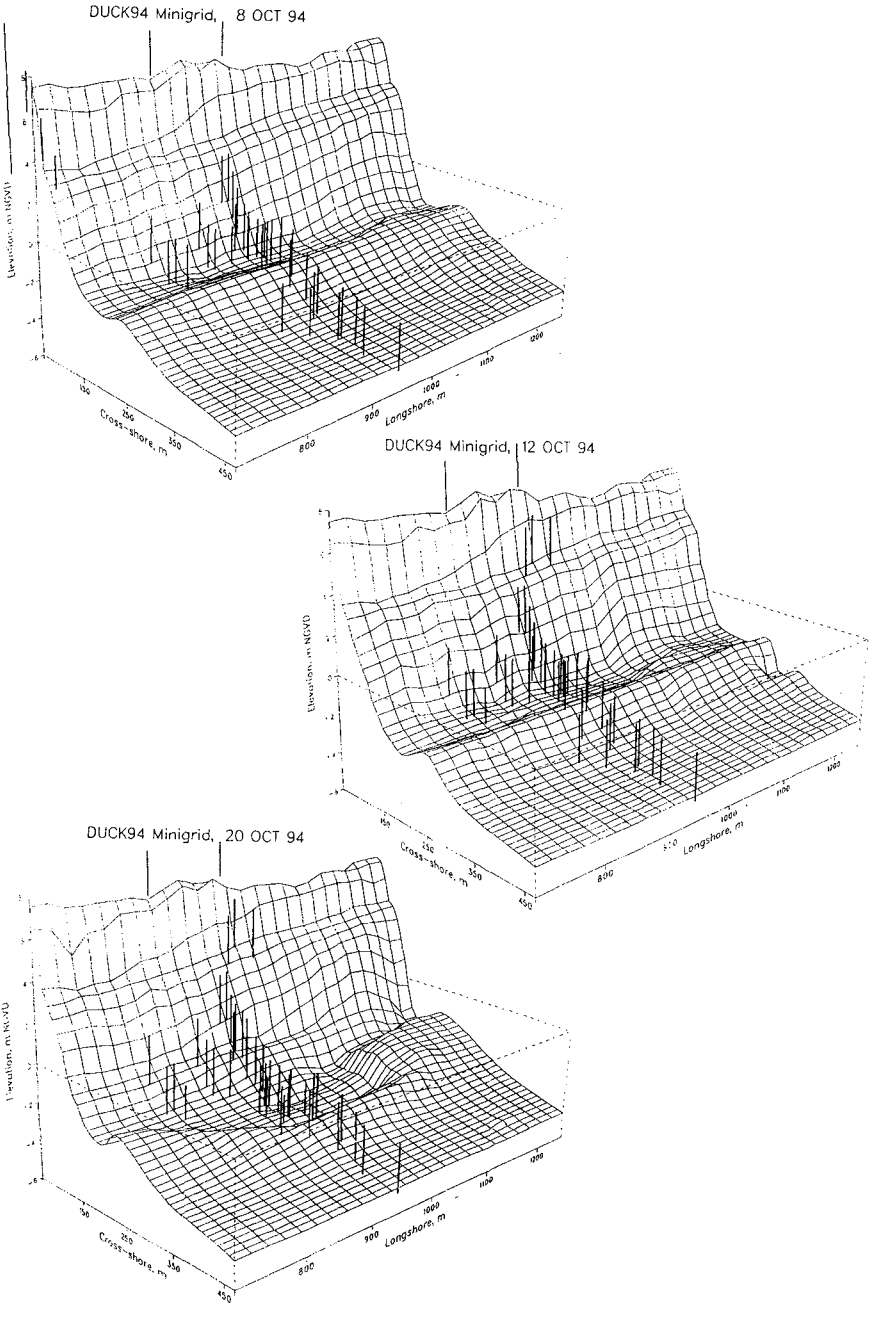

Figure 1. Three-dimensional bathymetry profiles of the survey area as mapped by the CRAB for the three days considered (Oct. 8, 12, and 20).

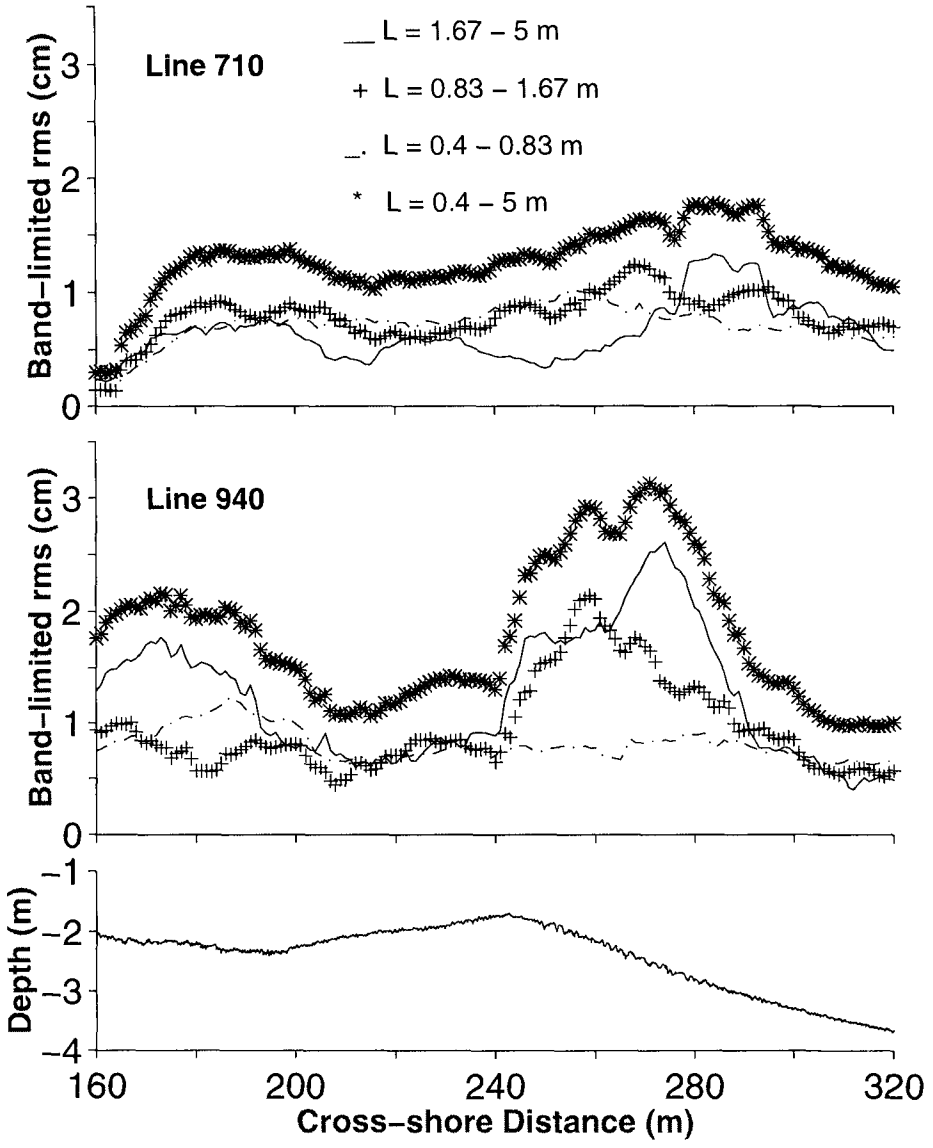

Figure 2. Band limited rms heights calculated across lines 710 (upper panel) and 940 (middle panel) for Oct. 8. Combined CRAB and altimeter bathymetry profile of line 940 for Oct. 8 (lower panel).

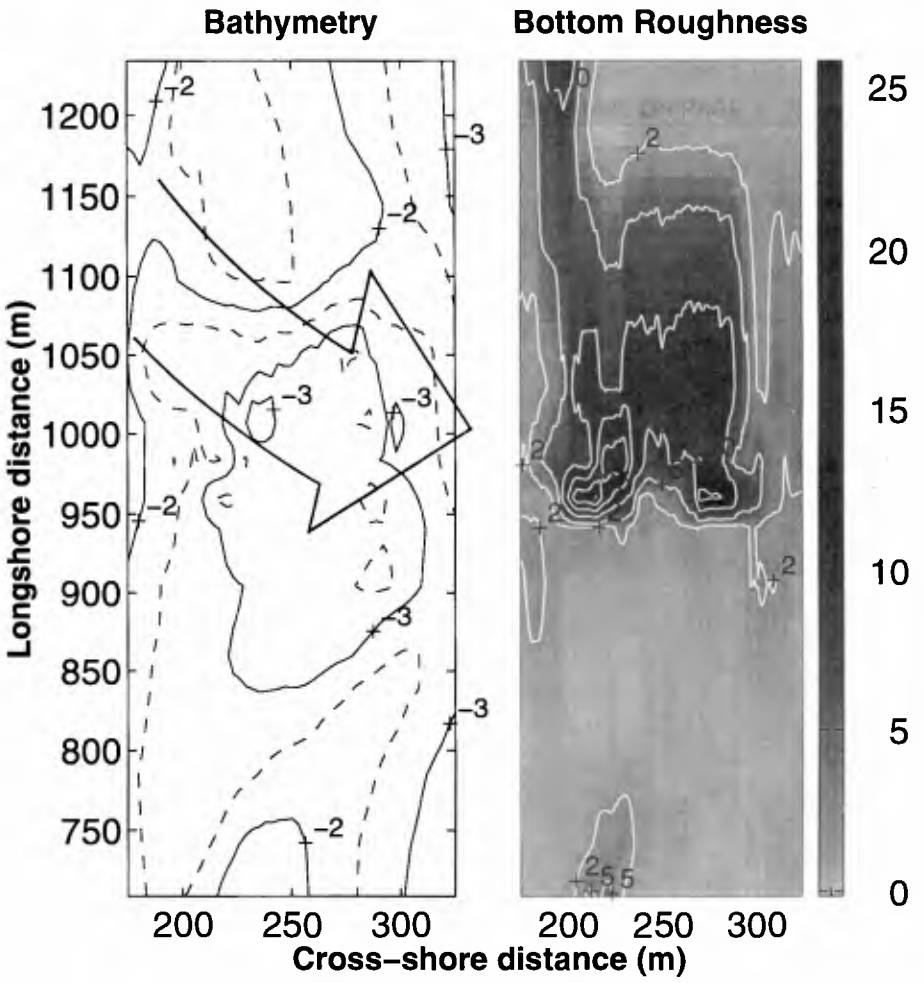

Figure 3. Bathymetry contour plot of DUCK94 survey area for Oct. 20 (left plot). Contour levels are in meters. Rip current is qualitatively indicated based on dye observations. Bottom rms roughness contour plot of survey area for Oct. 20 (right plot). Contour levels are in centimeters.

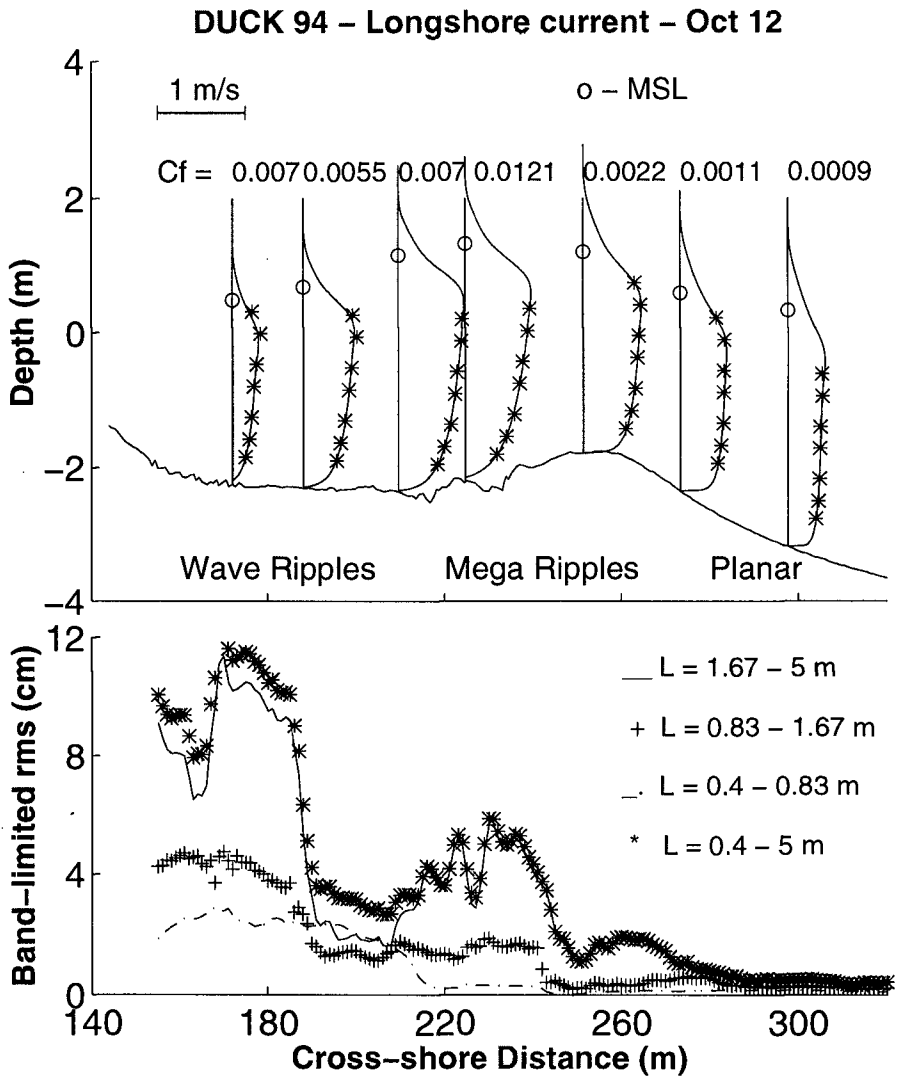

Figure 4. Vertical profiles of mean longshore currents superposed on bottom profile with tide elevation indicated by (o) and measured C_f values (upper panel). Variation of band-limited rms bottom roughness with the cross-shore distance for Oct. 12 (lower panel).

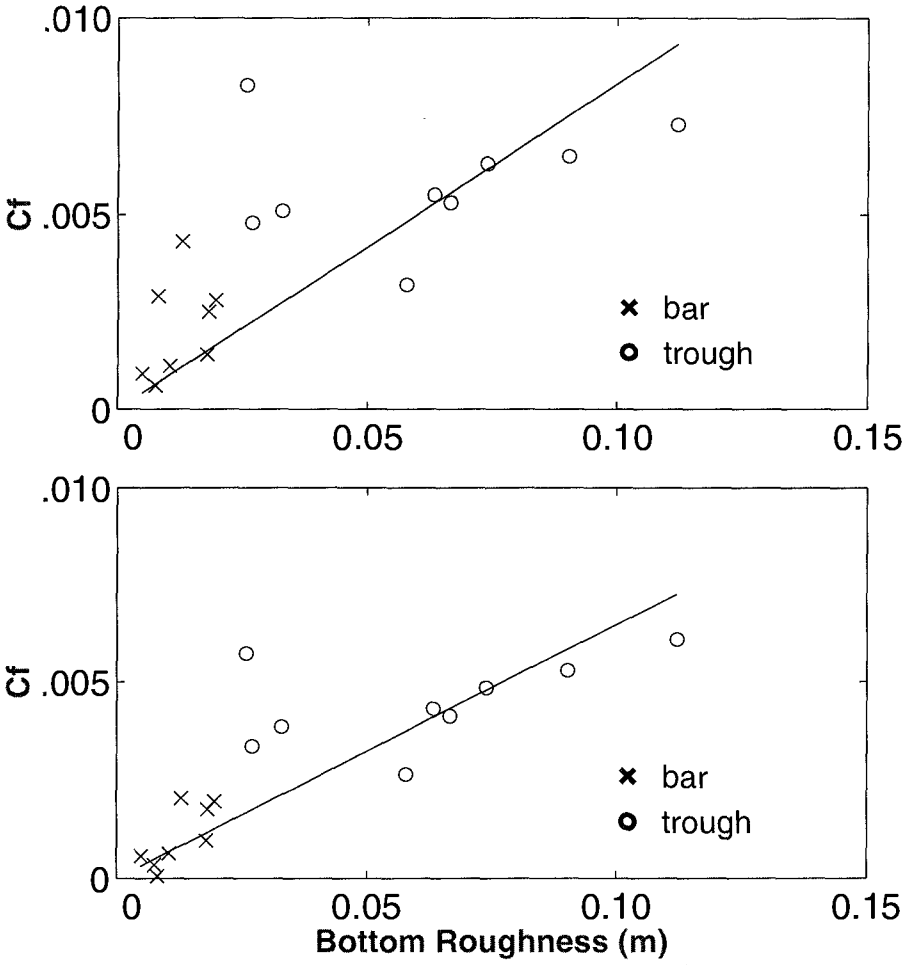

Figure 5. Total bed shear stress (C_f) versus bottom roughness (upper panel). The line represents a linear regression with a regression eoefficient of 0.68. Bed shear stress coefficient without skin friction contribution (C_f') versus bottom roughness (lower panel). The line represents a linear regression with a regression coefficient of 0.80.